

mmWave on a Farm: Channel Modeling for Wireless Agricultural Networks at Broadband Millimeter-Wave Frequency

Shuai Nie*, Mohammad Mosiur Lunar*, Geng Bai†, Yufeng Ge†,
Santosh Pitla†, Can Emre Koksal‡, and Mehmet C. Vuran*

*School of Computing, University of Nebraska-Lincoln, Lincoln, NE 68588, USA

{shuainie, mcv}@unl.edu

†Department of Biological Systems Engineering, University of Nebraska-Lincoln, Lincoln, NE 68583, USA

‡Department of Electrical and Computer Engineering, Ohio State University, Columbus, OH 43210, USA

Abstract—Millimeter-wave (mmWave) spectrum promises high throughput links for next-generation wireless agricultural networks, which will be characterized by teams of autonomous ground vehicles, unmanned aerial vehicles (UAVs), and connected agricultural machinery. However, channel models at mmWave frequencies in agricultural environments remain elusive. Moreover, due to the dynamic crop growth behavior, agricultural field channels bear notable distinctions from urban and rural macrocellular network channels. In this work, the most extensive agricultural field experiments on the mmWave spectrum are reported and a channel model is developed to characterize the large-scale path loss, coherence bandwidth, and link quality under the effect of various environmental factors. In particular, this study investigates the effects of wind on signal-to-noise ratio, and the diffuse scattering of electromagnetic waves due to near-canopy propagation at different crop growth stages. Accordingly, (1) during the growing season, the crop canopy surface acts as a “new ground”. This new ground creates multipath components and results in a higher path loss exponent, which is correlated with the relative height between the crop canopy surface and the radios, (2) An increase of 4 m/s in gust speed results in a half-power drop (3-dB SNR degradation) due to beam misalignment and increased scattering, (3) the channel coherence bandwidth increases as the water content in the crop decreases, and (4) the beam-level spatial consistency allows for micro-mobility support for agricultural robotic applications. It is also shown that the impacts of humidity and water vapor on the mmWave channel are insignificant in the absence of rain and irrigation. Such characteristics are fundamental for designing advanced channel estimation and signal processing algorithms in advanced agricultural Internet-of-Things solutions. The extensive experiment dataset is made public for future reproducible research (<https://ieeegapport.org/documents/mmwave-farm-channel-modeling-wireless-agricultural-networks-broadband-millimeter-wave>).

Index Terms—Millimeter-wave, agricultural propagation channel, path loss, delay spread, crop growth stages.

I. INTRODUCTION

Wireless communication systems have evolved significantly over the past several years. In sharp contrast to the multi-gigabits-per-second (Gbps) that 5G has achieved in urban areas, the rural wireless networks still suffer from a massive gap in connection speed, with some areas not even covered by wireless infrastructure [1]. This digital divide will exacerbate

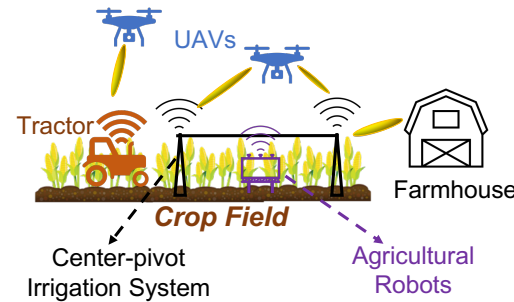


Fig. 1: Future smart agricultural networks with ubiquitous connectivity.

as more research focuses on developed areas with higher user densities. The recent advances in sensing, automation, and digitization in agriculture have led to a new vertical, agricultural Internet of Things (Ag-IoT), for the 5G systems and emerging 6G systems [2]. Emerging applications such as precision farming and digital agriculture suggest a solid motivation to equip traditional farming practices with advanced communication and computing capabilities [3]. The Ag-IoT will include smart farming equipment, which requires broadband connectivity [4]. Recent innovations in autonomous field robots will also increase these requirements to multi-Gbps throughput levels for joint multispectral sensing and autonomous driving tasks [5], requiring high throughput solutions in the fields such as millimeter-wave (mmWave) technology [6]. However, behaviors of mmWave links in typical agricultural settings are not well known.

Traditional microwave frequencies (sub-6 GHz) have been used in rural macrocellular networks. Even though the benefits include better coverage, readily available commercial systems, and mature and less sophisticated signal processing techniques, these frequency bands have been heavily utilized by various wireless systems, including the global positioning system (GPS) and traditional cellular networks. However, the limited bandwidth does not permit higher data rates, a prerequisite to achieving high spectral efficiency, a key driving force for next-generation wireless system design for the agricultural scenario. As shown in Fig. 1, next-generation agricultural

networks will require ubiquitous connectivity between data-hungry devices, including tractors, UAVs, agricultural robots, center-pivot irrigation systems, and farmhouses. In this way, a communication network with high throughput can be established among these smart agricultural infrastructures with emerging agricultural ground robots and unmanned aerial vehicles (UAVs) to efficiently deliver a large amount of data collected from crops and soil (e.g., phenotyping data).

Recognizing the deficiencies in conventional sub-6 GHz wireless systems for future agricultural communication development, it is necessary to seek new frequency bands to tackle the challenges of limited spectral efficiency and high interference. To this end, millimeter wave (mmWave) has become a promising candidate for urban areas and massive rural regions to bridge the digital divide. Some of the mmWave spectrum (28–47 GHz) has been officially adopted in the 5G New Radio (NR) as part of a global standard in radio access technology [7]. Part of the V-band spectrum at 60 GHz has also been extensively utilized in short-range indoor scenarios. At 60 GHz, there is a total 7 GHz available bandwidth, which will alleviate the spectrum crunch issue.

In this work, we investigate the propagation channels in rural agricultural fields with two types of crops and at different crop growth stages. The aim is to understand how the mmWave channel is subject to (1) environmental factors, such as wind, and (2) crop growth (i.e., obstruction of the first Fresnel zone between transceivers). The contributions of this work are:

- The most extensive set of channel measurements at the mmWave spectrum to date is conducted in three farm fields during the growing season of two crop types over a period of five months, with over 6,860 data points collected. Each data point contains a series of measured parameters, including beam indices, signal-to-noise ratio, and received signal strength indicator. To the best of our knowledge, this is the most extensive dataset on mmWave agricultural channels. We also make the dataset public¹.
- From measurements conducted under different wind conditions, we characterize the link stability with respect to different wind/gust speeds.
- We analyze the path loss statistics from measurements and investigate the correlation between link performance and environmental factors (e.g., water content levels in crops and water vapor density in channels), and types of crops (i.e., corn and soybean).
- From the measured channel impulse response, we analyze the channel delay spread and the relationships between coherence bandwidth and crop growth dynamics.
- Regarding the relative heights between crops and transceivers, we analyze the effects of ground reflection and near-canopy propagation based on the two-ray ground reflection model and the first Fresnel zone model.

The rest of this paper is organized as follows. The related work is discussed in Sec. II. The measurement campaign and

methodology are described in Sec. III. Relevant background in rural agricultural channels and agricultural practices is presented in Sec. IV. The mmWave agricultural channel model and an analysis of the impacts of crop height, crop type, water content, wind and gust, and water vapor on communication are presented in Sec. V. Finally, the paper is concluded in Sec. VI.

II. RELATED WORK

Previous research on rural wireless channel modeling macrocellular scenarios at microwave frequencies. For example, 3GPP TR 38.901 Release 16 [8] predominantly considers a rural macrocellular (RMa) scenario with frequencies up to 7 GHz. More specifically, the height of the base station is considered to be at least 35 m (i.e., on a tower), and the scenario is considered with 50% user equipment in indoor spaces and 50% in a car. These parameters and assumptions imply that users are either in rural residential houses or traveling in vehicles, which neglects the emerging communication scenario, namely, the Ag-IoT [2]. With respect to rural channel propagation modeling, limited measurements and network planning efforts have been reported at various frequencies. In particular, the measurements, which were performed in rural Virginia at 73 GHz to study the rural macrocellular channel, demonstrate an achievable range of more than 10 kilometers under clear weather [9]. Another channel model focuses on characterizing the near-ground propagation with obstruction and power margin design for broadband rural wireless networks [10].

So far, existing research effort related to rural *agricultural fields* is solely found in the Internet of Things (IoT). A near-ground propagation channel is proposed to discern dominant path behavior based on the Fresnel zone break distance [11]. Although proved accurate, this model does not consider the potential impact cast by various soil and crop features. To characterize the properties of soil and crops at different growth stages, remote sensing approaches have been widely adopted [12]. The channel responses back-scattered from crop canopies and soil captured by the remote sensing satellite are utilized to quantify the soil moisture level, crop canopy biomass, and surface roughness, respectively [13]. The wireless underground channel is characterized in Ag-IoT scenarios in terms of path loss and coherence bandwidth [14]–[16]. However, existing studies are limited to the RMa scenario, thus not directly applicable to understanding the propagation channel for smart agriculture at mmWave frequencies.

With current research efforts in rural wireless networks focusing on coverage analysis for conventional user groups, characterization of crops' physical and chemical properties based on remote sensing techniques, and near-ground channel modeling in wireless sensor networks, there is a lack of in-depth knowledge about propagation channel in agricultural fields that captures the dynamics of crops during the growing season in the mmWave spectrum. To the best of our knowledge, our study, based on extensive measurements [17], is the first one that bridges this research gap, which is critical for designing a smart agricultural network paradigm. The measurements were designed considering an agricultural

¹<https://ieee-dataport.org/documents/mmwave-farm-channel-modeling-wireless-agricultural-networks-broadband-millimeter-wave>

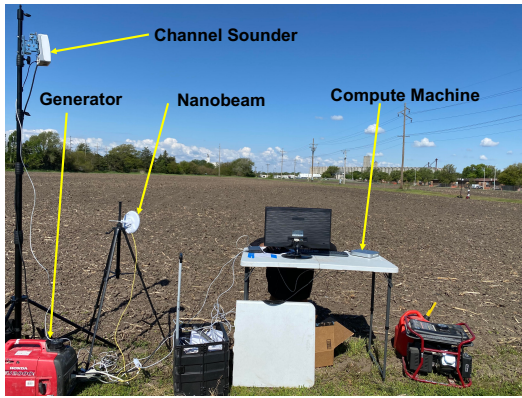


Fig. 2: The channel sounding system setup.

small cell scenario, which is envisioned for smart agriculture applications. This small cell scenario is distinct from the traditional rural macrocellular network settings. Therefore, channel characteristics from the conventional macrocellular scenario are not applicable due to the natural dependence of channel statistics upon frequency and distance under analysis.

III. MEASUREMENT CAMPAIGN AND METHODOLOGY

To understand the mmWave agricultural channels thoroughly, an extensive measurement campaign was conducted in three fields at two research farms.

A. Wireless Channel Measurement System and Procedure

A pair of TerraGragh (TG) mmWave channel sounders [18] that transmit and receive the IEEE 802.11ad waveform at the V-band is used for the experiments. As shown in Fig. 2, the system setup follows the best principles from the Telecom Infra Project (TIP) project [19]. Specifically, the TG sounder operates at a center frequency of 60.48 GHz with an 8×36 phased antenna array at each node, with a half-power beamwidth of 2.8° and 12° in the azimuth and elevation plane, respectively. The nominal effective isotropic radiated power (EIRP) is around 36 dBm. Other parameters of the channel sounder are listed in Table I.

TABLE I: Channel Sounder Parameters [18]

Parameter	Value
Center frequency	60.48 GHz
Bandwidth	2.16 GHz
Antenna array size	36×8
EIRP of Tx	36 dBm
3-dB beamwidth (azimuth)	2.8°
3-dB beamwidth (elevation)	12°
Beam sweeping step (Tx & Rx)	2.8°
Sweeping range (azimuth)	$\pm 45^\circ$

The TG sounder is equipped with several measurement modes, including an extensive beam sweeping mode (in the azimuth plane ranging from -45° to $+45^\circ$ with a step size of 2.8°) and a live channel sounding mode that captures the channel impulse response (CIR) in real-time. The measurement steps are the following: At each fixed Tx and Rx location, first, beam sweeping is performed for a total of 4,906 beam pairs from each of the 64 distinct beams at both Tx and Rx [18],

[19]. Then, the best beam pair with the maximum signal-to-noise ratio (SNR) is selected from all beam pairs with a valid received signal. Finally, this best beam pair is used for live channel sounding measurements to record the CIR.

The experiments are conducted in two research farms: the Eastern Nebraska Research, Extension and Education Center (ENREEC) Field Phenotyping Facility² near Mead, Nebraska and the Rogers Memorial Farm (RMF)³ near Lincoln, Nebraska as shown in Fig. 3. In particular, at the ENREEC site, four link distances ranging from 19.2 meters (m) to 77 m were used in a corn field (Fig. 3a). At RMF, two adjacent fields with corn and soybean were used to measure propagation channel at distances ranging from 50 m to 112 m (Fig. 3b). For each experiment, transmitter and receiver heights are set to 1.83 m/6 ft, 2.44 m/8 ft, and 3.05 m/10 ft, where applicable⁴. A detailed list of experiment configurations can be found in Table II. The measurement locations are marked, and the same measurements are repeated over a period of five months. When the crop canopy exceeds the transmitter-receiver height, it is observed that the mmWave signals cannot propagate through the crop canopy, and a link cannot be established. Therefore, certain Tx/Rx heights are not repeated when the crop canopy height exceeds these heights.

The measurement procedure provides the following benefits: (1) The extensive beam sweeping provides CIRs to reconstruct the channel across different beam pairs, thus providing information to model the channel, especially the beam-level spatial consistency with multipath components (as will be discussed in detail in Sec. V-E). (2) From the collected CIRs and the root-mean-square (RMS) delay spread, we can identify the cause of multipaths (e.g., ground/soil reflection or scattering off of crop canopy) based on the difference in path travel distance compared with the line-of-sight (LOS) path. (3) Due to the very narrow beamwidth of the nodes and long separation distances in the field, it is not easy to achieve a perfect beam alignment even with careful calibration. Hence, the beam sweeping followed by the best beam pair selection guarantees a well-aligned pair of beams along boresight. (4) The path loss values calculated in the live channel sounding mode allow us to characterize the large-scale path loss statistics, which are crucial in channel modeling. (5) The SNR values from the live channel sounding mode are useful to analyze the link stability under channel dynamics at different growth stages.

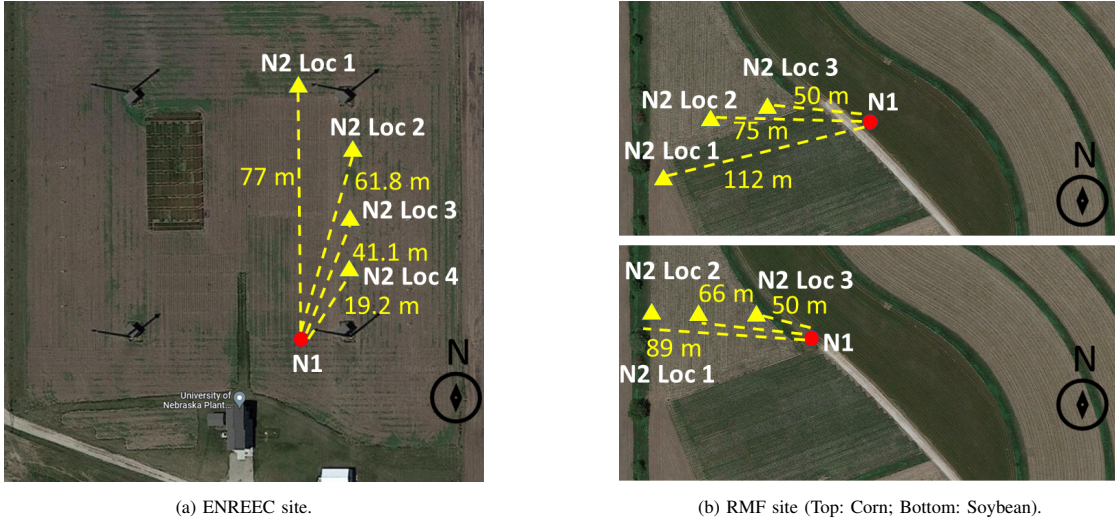
B. Weather Data

At ENREEC, a weather station collects weather and environmental parameters, including air temperature (T_a) and relative humidity (2 m above the ground), precipitation, wind speed, gust speed and direction (3 m above the ground), photosynthetically active radiation, and total shortwave radiation. These variables are recorded as one-minute interval averages. The weather station also records maximum wind (gust) speed

²<https://ard.unl.edu/phenotyping/field-phenotyping-facility>

³<https://bse.unl.edu/rogers-memorial-farm>

⁴These heights were measured in feet in the field but the SI unit of meters was used in data processing and denotation.



(a) ENREEC site.

(b) RMF site (Top: Corn; Bottom: Soybean).

Fig. 3: Satellite images of the two experimental sites (Source: Google Maps).

TABLE II: Experiment details with crop type, crop & measurement heights, and measurement distances.

Date	Location	Crop type	Crop height [ft]	Measurement heights [ft]	Link distances [m]
July 7	ENREEC	Corn	4.7	6, 8	77
July 16	ENREEC	Corn	6.8	8, 10	19.2, 41.1, 61.8, 77
Sept. 23	RMF	Corn	7.9	8, 10	112
Sept. 28	RMF	Corn	7.9	8, 10	75
Oct. 7	RMF	Corn	7.9	8, 10	50
Oct. 8	RMF	Soybean	2.2	8, 10	50, 66, 89
Oct. 12	ENREEC	Corn	7.9	8, 10	77
Nov 16	ENREEC	Empty	1.6 (corn stubble)	8, 10	19.2, 41.1, 61.8, 77
Nov 23	RMF	Empty	1.6 (corn stubble) & 0	8, 10	50, 66, 75, 89, 112

within a one-minute interval with a sampling rate of five seconds. These weather parameters are utilized to analyze the impacts of wind, gust, and humidity on channel performance during and between experiments.

C. Data Analysis

The TG sounder provides the received power, path loss, EIRP, RMS delay spread, CIR, and SNR. In addition, channel parameters including coherence bandwidth, path loss exponent, and standard deviation in shadowing are calculated based on the collected data. The agricultural field propagation channels at mmWave frequencies have unique characteristics regarding their intrinsic relations with the crops and environmental variables. For example, the wavelength (≈ 5 mm) is comparable to the size of the tip of crop leaves, which leads to a unique scattering environment. Similarly, the wind and the growth stages of the crop may impact the channel properties. We analyze the experimental data under the following conditions to explore these relations.

Wind/Gust: Even though the wind does not affect electromagnetic wave radiation in a free-space channel, it might perturb the link stability by affecting nearby scatterers and the endpoints. Thus, at the ENREEC site, we analyze the experiments in a maize field under windy weather (July 7 and Nov. 16) and mild weather (July 16). It is worth mentioning that these periods capture different stages of growth: early July (the fourteenth-leaf stage, or V14⁵) and November (after



(a) Crop canopy in early July at the V14 stage.



(b) The rough surface of the soil after harvest in November. The height of the stubble is around 0.5 m.

Fig. 4: Two types of surface roughness on different experiment days.

harvest), as illustrated in Fig. 4.

Crop Growth: Crop growth is a unique factor that distinguishes the agricultural field propagation channel from that in urban or rural macrocellular networks. To study the effects of

⁵<https://cropwatch.unl.edu/2021/2021-corn-yield-forecasts-july-14>

partial blockage by the crops and a potential “ground effect” created by the canopy surface, we analyze experiment data from different crop growth stages in ENREEC. In addition, experiments performed after harvest are included as a control.

Since the sets of experiments were stretched on different days over five months to capture the dynamics in crop growth, different weather conditions, such as temperature, relative humidity, air pressure, and wind speed, were also naturally included in the collected data, which may contribute as a set of factors that affect the received signal. Therefore, for a fair comparison to determine the correlation between the rural agricultural field channel and a particular environmental factor, we tried our best to maintain other factors consistent from a subset of experiments. It is found that the wind speed and humidity are not correlated ($R^2 < 0.1$) during the experiment dates and can be considered independent factors. In particular, we compare the data reported with a fixed 77-m link distance in July and November to draw a fair comparison under different wind conditions. The coherence bandwidth comparison result is also made upon reported data in July, October, and November at a 77-m link. In contrast, the large-scale path loss results are drawn from all data collected from various distances ranging from 19.2 m to 77 m. The above analysis concerning a single crop type’s different growth stages is based on data collected from the ENREEC site. In contrast, a comparison between two different crops (i.e., corn and soybean) utilizes data from the RMF site.

IV. BACKGROUND

The domain knowledge from agricultural practices is essential to understanding and analyzing channel dynamics. In this section, we discuss the metrics that quantify the agricultural channels in terms of the unique propagation environment, leaf area index, the water content of crop leaves, and humidity.

A. Agricultural Propagation Environment

The rural wireless networks bear several distinctions from their counterparts in the urban and indoor scenarios in the following ways. First, the physical environment of a rural area differs remarkably from that of an urban area. Instead of tall buildings, light pole infrastructures, and vehicles, the agricultural fields consist of crops and infrastructures such as farmhouses, grain bins, and field vehicles such as seeders, combines, tractors, and center pivot irrigation systems. As a result, the characteristics of rural wireless channels differ significantly from those in the urban scenario. Second, partial LOS path obstruction—most typically crops—can impair signal propagation. All these components impact the link quality in rural propagation channels. The ITU’s current vegetation model [20] only concerns links *through* tree canopies, which does not apply to rural scenarios where *partial LOS path obstruction* is more prevalent in crop fields. Third, the rural wireless networks in agricultural fields experience a dynamic and seasonal demand. In other words, during the growing season, varying heights and water contents of crops will alter the composition of the propagation environment. Therefore,

the characterization of the mmWave channel in agricultural fields has a vital role in analyzing this peculiar environment as a foundation for designing advanced upper-layer solutions.

B. Leaf Area Index

Leaf area index (LAI) is the ratio between the one-sided green leaf area and unit ground surface area, which ranges from 0 (i.e., bare ground) to 6–7 (i.e., peak growth season) for corn and soybean. The peak LAI is reached in the middle of the season when the green vegetation is at maximum. LAI will decrease when the crop starts to mature later in the season. LAI is highly sensitive to the varieties, water management (e.g., irrigated vs. dryland), and nutrient management. From the dates of field experiments, the LAI values are 3.14 in early July and 4.88 in mid-July for corn, 2.51 in early July, and 7.58 in mid-July for soybean, respectively. When the LAI is high, the top view of the ground surface is covered by a crop canopy, which can be considered as a “new ground” that varies over growth stages, as shown in Fig. 4a. Thus, when considering signal reflection, the characteristics of crop canopies should be taken into account to yield a precise model.

C. Water Content in Crop Leaves

Water content in crop leaves is highly correlated with growth stages. The corn has an average value of 72.3%, with a standard deviation of 2.7% during the growing season. The estimated water content is significantly lower in October ($\sim 35\%$ ⁶). Soybean has a leaf water content of 80.7% and a standard deviation of 2.32% during the growing season. As the crops enter the reproductive stage and mature (in late season), the leaf water content decreases substantially, similar to the LAI behavior.

D. Atmospheric Gases

The attenuation of RF signals by atmospheric gases is mainly due to oxygen and water vapor molecules. In our study, we adopt the ITU model Recommendation ITU-R P.676-12: Attenuation by atmospheric gases [21]. The water vapor density can be derived from the water vapor pressure P with the molecular mass of water based on the ideal gas law as $PV = NRT$, where N is the amount of substance, V is the volume, $R = 8.3145 \text{ J} \cdot \text{mol}^{-1} \cdot \text{K}^{-1}$ is the molar gas constant, and T is the temperature (it is assumed to be 303 K in July and 293 K in November). The water vapor density is

$$\rho = \frac{MP}{RT} = \frac{M}{RT} \frac{RH}{100} e^0(T_a), \quad (1)$$

where $M = 18 \text{ g/mol}$ is the molecular mass of water, $e^0(T_a) = 0.6108 \exp\left(\frac{17.27T_a}{T_a + 237.3}\right)$ is the reference air vapor pressure in kPa, T_a is the temperature in Celsius, and RH is the relative humidity measured by the weather station. The right-hand side of (1) is derived by replacing P with $e^0(T_a)RH/100$ [22].

⁶<https://crops.extension.iastate.edu/blog/brian-hornbuckle-richard-cirone/corn-water-stress-observed-reduced-moisture-content>

TABLE III: PLE and standard deviation of shadowing with link range in [19.2, 77] m of best beams in a corn field at various relative heights at ENREEC.

ΔH [ft]	n	σ [dB]	h_t/r [ft]	d_F [m]	$d_{2\text{ray}}$ [m]	Date
0.1	2.35	1.6	8	0.8	2.4	10/12/21
1.2	1.95	1.5	8	108.0	339.2	07/16/21
1.3	2.00	2.3	6	126.7	398.0	07/07/21
2.1	1.96	0.8	10	300.0	942.1	10/12/21
3.2	1.95	1.8	10	767.7	2,411.7	07/16/21
3.3	1.96	2.1	8	816.4	2,564.8	07/07/21
4.4	1.88	0.3	6	1,451.4	4,559.7	11/16/21
6.4	1.85	0.9	8	3,070.7	9,647.0	11/16/21
8.4	1.91	1.4	10	5,289.8	16,618.4	11/16/21

V. CHARACTERIZATION OF MMWAVE AGRICULTURAL FIELD CHANNELS

Based on the collected data from experiments, the characterization of agricultural fields at mmWave includes (1) modeling of the large-scale path loss at different crop growth stages, (2) comparison of large-scale path loss statistics between different types of crops, (3) analysis of the channel's coherence bandwidth at different crop growth stages, (4) analysis of link stability under wind effect, and (5) comparison of signal attenuation by atmospheric gases at different field seasons. This data is made available in the public repository of the IEEE dataport.

A. Large-scale Path Loss Modeling

In wireless propagation channels, the large-scale path loss can be expressed as [23]:

$$\text{PL} = \text{PL}_0(d_0) + 10n \log_{10} \left(\frac{d}{d_0} \right) + A_{\text{air}} + \chi_{\sigma}, \quad (2)$$

where $\text{PL}_0(d_0)$ represents the free space path loss at a reference distance $d_0 = 1$ m, n is the path loss exponent (PLE), A_{air} is the attenuation caused by atmospheric gases, which are dominated by oxygen and water vapor molecules suspended in the air, and χ_{σ} is the shadowing factor with a standard deviation, σ . In our study, we choose the close-in free space reference distance d_0 as 1 m, which has a free space path loss of $32.4 + 20 \log_{10}(f)$ dB at the center frequency $f = 60.48$ GHz [23]. Hence, (2) can be simplified as

$$\text{PL} = 32.4 + 20 \log_{10}(f) + 10n \log_{10}(d) + A_{\text{air}} + \chi_{\sigma}, \quad d \geq 1 \text{ m}. \quad (3)$$

Based on this model, we can set a fair baseline to compare path loss obtained from different link distances and under different crop growth stages. Table III shows the computed n (the 2nd column) and σ (the 3rd column) values under different measurement dates. This table is sorted by different relative radio-canopy surface height, ΔH , values in the 1st column, which aims to indicate the correlation between path loss and crop growth stages. The Tx/Rx height measured above the ground surface is listed in the 4th column.

B. A “New Ground” – Canopy Surface

From Table III and Fig. 5, it can be observed that the PLE is negatively correlated with ΔH . For example, when the crop

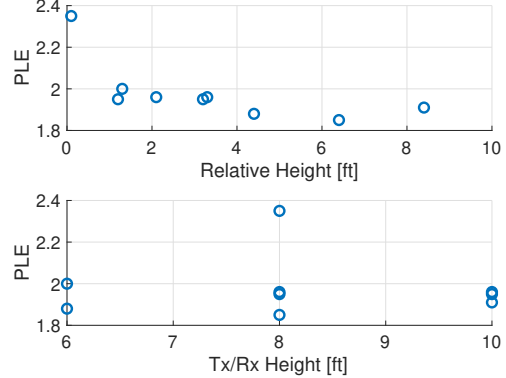


Fig. 5: Upper: A clear correlation is shown between PLE and relative radio-canopy height: as relative height decreases, the path loss exponent increases. Lower: No strong correlation exists between PLE and absolute heights of Tx and Rx in different crop growth stages.

is almost at the same height as the TG sounder at 8 ft (1st row in Table III), the PLE has the highest value of 2.35 even under LOS propagation with the best-aligned beam pair. This value is much higher than the case with the same TG sounder height, but $\Delta H = 6.4$ ft (2nd to 9th row in Table III). The results prove that **the crop canopy acts as a new ground surface that reflects or scatters signals**, as illustrated in Fig. 6. As the relative height increases, the PLE decreases and fluctuates around the theoretical value of $n = 2$ under the LOS scenario. The PLE computation in this work uses the *best beam pair* only, which is different from the preliminary approach in [17] that uses a *main beam region* considering a slightly wider angular range.

To further understand this near-canopy propagation phenomenon, we analyze the Fresnel zone model and two-ray ground reflection model in-depth. The near-canopy propagation leads to the obstruction of the first Fresnel zone, where ground reflection contributes to signal attenuation and free space path loss. This break distance, d_F , and the two-ray ground reflection break distance, $d_{2\text{ray}}$, are both related to transceiver heights and approximated as [11], [24]:

$$d_F \approx \frac{4\pi h_t h_r}{\lambda}, \quad d_{2\text{ray}} \approx \frac{4\pi h_t h_r}{\lambda}, \quad (4)$$

where h_t and h_r are the heights of the Tx and Rx with respect to the ground in a general sense, respectively. Therefore, before harvest, this height (equi-height for both Tx and Rx) represents the height difference between Tx/Rx and crop canopy surface. The two types of break distances are also listed in Table III in the 5th and 6th columns, respectively. Depending on the relative heights and link distances, we categorize the scenario into three groups:

1) $d < d_F$: When the link distance is less than the break distance of the first Fresnel zone, the mean path loss is equivalent to the LOS free space path loss, which is due to the spreading loss of the wavefront. From Table III, all rows, except the first one, comply with this criterion, and their PLE values are also less or equal to the LOS free space PLE.

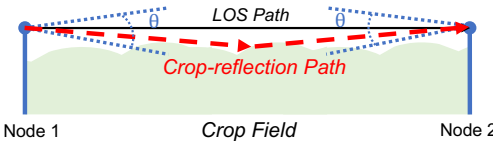


Fig. 6: Illustration of field link geometry. The black line denotes the LOS path, and the red dash curve represents the reflected path from the crop canopy (shown as the green cluster). Each node has a half-power beamwidth of $\theta = 12^\circ$ in the elevation plane.

TABLE IV: Wind speed information from field measurements.

Date	Ave. [m/s]	Max. [m/s]	Min. [m/s]
07/07/21	4.0	5.1	2.3
07/16/21	2.0	2.5	1.4
11/16/21	6.2	7.5	2.5

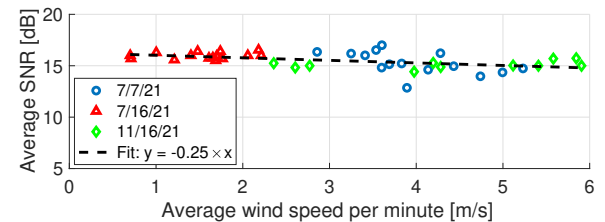
2) $d_F \leq d < d_{2\text{ray}}$: When the link distance is greater than the break distance of the first Fresnel zone, the obstruction leads to higher path loss, which is visible from a larger PLE and higher standard deviation in shadowing.

3) $d \geq d_{2\text{ray}}$: When the link distance is greater than the break distance of the two-ray ground reflection model, the path from ground reflection and LOS path are the dominant paths that interfere with each other, leading to a much greater path loss. The first row in Table III falls into this category, and the PLE value is also the highest. Based on the LAI analysis in Sec. IV-B, this “ground reflection” is due to signals reflected off the crop canopy surface.

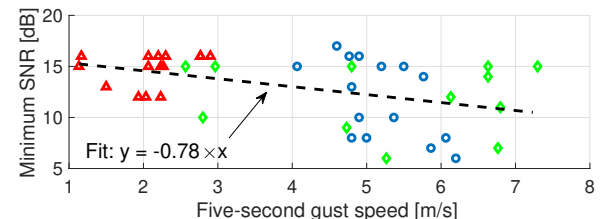
C. Wind Effects on Link Stability

Our characterization of the wind effect on wireless links is based on the wind and gust speed data collected by a state-of-the-art weather station at the ENRECC site, which provides two types of data: the maximum five-second gust speed within a minute and the average wind speed measured over a minute. Specifically, three sets of data were collected from the same corn field and transceiver configuration on three days (July 7, July 16, and November 16) with distinct wind conditions, according to the Beaufort scale [25], a widely utilized reference for the empirical measure of wind speed. The wind speed statistics are shown in Table IV. The first set of measurements was conducted under a gentle breeze (Level 3 on the Beaufort scale). In contrast, the second set of measurements was performed under the range from light air to light breeze (Levels 1 and 2), and the third set of measurements was conducted under light breeze to moderate breeze (Levels 2 to 4). Based on the real-time SNR values captured and recorded in the channel sounder, we obtain a one-on-one mapping between the SNR and wind speed statistics to characterize the impacts of wind on rural agricultural link stability at mmWave.

The correlation between wind speed statistics and SNR is shown in Fig. 7. In particular, in Fig. 7a, the 1-min average SNR is shown w.r.t. the 1-min average wind speed. It can be observed that a moderate gentle breeze leads to approximately 3 dB loss in average SNR. In Fig. 7b, the worst-case impacts of gust are shown, where the minimum SNR value obtained



(a) 1-min average wind speed vs. average SNR.



(b) 5-sec gust speed vs. minimum SNR.

Fig. 7: Correlation between wind statistics and the SNR.

TABLE V: PLE and standard deviation of shadowing with link range in [50, 112] m in corn and soybean fields at RMF.

Crop Type	ΔH [ft]	n	σ [dB]	$h_{t/r}$ [ft]	Date
Corn	0.1	2.18	3.8	8	09/23/21
	0.1	2.12	4.0	8	10/07/21
	2.1	2.15	5.3	10	09/23/21
	2.1	2.04	4.8	10	10/07/21
	6.4	1.88	0.4	8	11/23/21
	8.4	1.88	0.5	10	11/23/21
Soybean	5.8	1.85	0.3	8	10/08/21
	7.8	1.96	2.1	10	10/08/21
	10	1.84	1.5	10	11/23/21

within the 1-min interval is compared to the maximum 5-sec gust speed within that interval. It can be observed that higher wind speed leads to more than 12 dB of SNR loss in the worst-case scenario, which can significantly affect the link stability. By fitting a linear regression model, the instantaneous impact of a five-second gust suggests a 3-dB SNR degradation each time the gust speed increases by 4 m/s.

The impacts of wind on the channel are twofold: Wind results in the sway of the transceivers, which may lead to beam misalignment. Furthermore, the stronger wind increases channel dynamics due to crops swinging. We observe that both factors play a role by analyzing the datasets from July 7 (blue circles) when crop canopy is present and from November 16 (green diamonds) after harvest. The negative trend in after-harvest SNR data with increasing gust speed suggests that beam misalignment is present. When the daily min-SNR vs. gust speed slopes of July 7 (-3.57) and November 16 (-0.18) are compared, a higher negative slope is observed for the channel with the crop. This suggests that crop swinging increases the impacts of wind on channel stability with increased scattering.

D. Effect of Crop Types on Path Loss

Different types of crops have distinct biological profiles, the most notable of which include heights and LAIs. At the RMF, two adjacent fields with corn and soybean provide a good platform with the same soil type to analyze wireless signal

propagation channels over them and their effects. As shown in Table V, in the first four rows in the corn field, both the PLE and shadowing values are notably higher than those in the control experiments in November, indicating more multipaths reflected off the corn canopy. On the contrary, the soybean field behaves similarly before and after harvest, implying that the soybean canopy acts similarly to bare ground and that the soybean canopy behaves more uniformly than corn.

E. Coherence Bandwidth

For wideband mmWave systems that employ antenna arrays to perform beamforming, it is important to acquire accurate channel state information (CSI) to ensure acceptable SNR values are maintained for good link quality. However, the cost of channel estimation is proportional to the number of antenna elements; hence, too frequent computation of CSI sacrifices the time allocated for data transmission. Therefore, an analysis of the channel's flatness becomes important to prescribe an appropriate overhead for channel estimation. The coherence bandwidth provides a good insight into the beamforming channel estimation cost. The coherence bandwidth with a 50% channel correlation is expressed as $B_c = \frac{1}{5\sigma_\tau}$, where σ_τ is the delay spread from measurement data.

In our experiments, the channel sounder provides the option for live measurements on a fixed pair of beams, which capture the channel impulse response. Since each beam has a narrow beamwidth of 2.8° in the azimuth plane, to analyze the channel's coherence bandwidth in a broader angular domain, we select the main beam region centering the best beam pair with $\pm 5^\circ$. We characterize the relationship between the coherence bandwidth and different crop growth stages through the measurement data. In particular, the statistics of coherence bandwidth for fixed-length (77 m) and fixed-height (10 ft) links are shown at three growth stages of corn in Fig. 8. It can be observed that the median coherence bandwidth is inversely proportional to the leaf water content. Before harvest, the coherence bandwidth is larger in October when the crop becomes sparse in the field due to the loss of water content (at 35%) compared with that in July when the water content is measured at 72.3%. Furthermore, due to limited multipath, the coherence bandwidth has the largest median value and smallest variation after harvest (in November).

Through beam sweeping, we also observe that the beam-level spatial consistency can be achieved even when the beam pair is not perfectly aligned. In Fig. 9 the channel impulse response of three exemplary beam pairs is shown⁷. The angle of departure (AoD) at the Tx is fixed at -5.6° , while the Rx performs a beam sweeping with different angles of arrival (AoAs) of 4.2° , 8.4° , and 9.8° . The three beam pairs are not perfectly aligned. Yet, the power delay profiles demonstrate a consistent LOS path within a cluster that also contains multipath components that arrive in close intervals (≈ 2 ns) due to crop canopy reflection. This beam-level spatial consistency indicates a stationary channel for micro-mobility

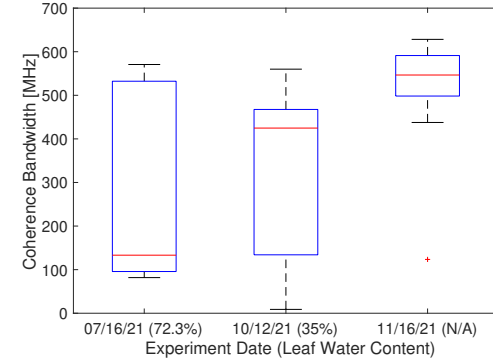


Fig. 8: Coherence bandwidth across different crop growth stages at a 77-m link with a fixed 10-ft Tx/Rx height. (Red bars: median values; Blue boxes: 25%-75% percentile, Black bars: minimum and maximum values; Red plus: an outlier. N/A: No leaf after harvest.)

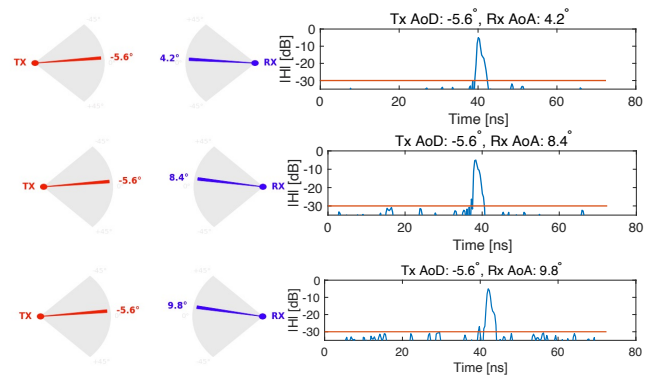


Fig. 9: Three exemplary beam pairs (left side) and impulse responses (right side, blue line). The red line in the figures on the right side shows the -25 dB threshold to distinguish significant taps. Neighboring beams observe spatially consistent channels with multipath components.

in agricultural robotic applications, which will be analyzed in depth in our future work.

F. Attenuation by Atmospheric Gases

The extensive path loss data from our experiments from July to November shows no correlation between water vapor density and the received power under clear weather and without irrigation practices. As shown in Fig. 10, the atmospheric gases do not cause a significant impact on path loss, as compared with free-space path loss. Even when the water vapor density shows a distinct difference in July and November, under clear days when no irrigation is performed, the term of A_{air} in (2) can be replaced with a predictable value shown in Fig. 10⁸. The impacts of irrigation and precipitation on power attenuation will be considered in our future work.

VI. CONCLUSIONS AND DISCUSSION

In this paper, we extensively analyze the mmWave channels in agricultural fields in terms of large-scale path loss, coherence bandwidth, and link quality under the effects of various

⁷The peak value is shifted by -5 dB for visualization purposes.

⁸MATLAB function *gaspl* adapted from an earlier version of [21] is used to compute the simulation result.

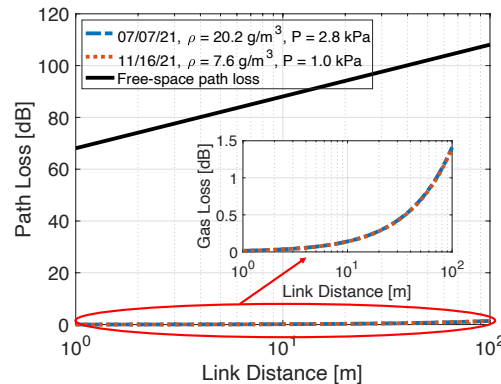


Fig. 10: Simulation results on atmospheric gases' attenuation to mmWave signal strength compared with free-space path loss.

environmental factors. Extensive field experiments over a period of five months were conducted to provide the largest mmWave agricultural channel dataset to make comparisons across different crop growth stages. In particular, we quantify the effects of wind and gust on the average and instantaneous signal-to-noise ratio, as well as the diffuse scattering of electromagnetic waves due to near-canopy propagation at different crop growth stages. From our analysis of large-scale path loss under different crop growth stages, we have shown that the **crop canopy surface acts as a “new ground”** that creates multipath components that result in higher path loss exponents during the growing season. Similarly, we show that the coherence bandwidth increases as the water content in the crop decreases. When comparing the path loss exponents at two types of crops, the soybean canopy is more uniform compared with the corn canopy, with much smaller values in path loss exponent and shadowing statistics. In our future work, these characteristics are essential to help us design advanced channel estimation and signal processing algorithms to bridge the digital divide in rural areas.

ACKNOWLEDGMENTS

This work is partly supported by NSF grants ECCS-2030272 and OIA-2044049. The authors would like to thank experiment site personnel D. Scoby (ENREEC), S. Hoff (RMF), and P. Jasa (RMF) for their support in conducting experiments at the corresponding sites. The authors also thank P. Subedi, D. Besonen, and S. W. Shin for their help in equipment setup and field measurements.

REFERENCES

- [1] Y. Zhang, D. J. Love, J. V. Krogmeier, C. R. Anderson, R. W. Heath, and D. R. Buckmaster, “Challenges and Opportunities of Future Rural Wireless Communications,” *IEEE Commun. Mag.*, vol. 59, no. 12, pp. 16–22, 2021.
- [2] M. C. Vuran, A. Salam, R. Wong, and S. Irmak, “Internet of underground things in precision agriculture: Architecture and technology aspects,” *Ad Hoc Networks*, vol. 81, pp. 160–173, dec 2018. [Online]. Available: <https://doi.org/10.1016/%2Fj.adhoc.2018.07.017>
- [3] Q. Yan, J. Lou, M. C. Vuran, and S. Irmak, “Scalable Privacy-Preserving Geo-Distance Evaluation for Precision Agriculture IoT Systems,” *ACM Trans. Sen. Netw.*, vol. 17, no. 4, jul 2021. [Online]. Available: <https://doi.org/10.1145/3463575>
- [4] Deere and Company, “Deere and Company Comments on Inquiry Concerning Deployment of Advanced Telecommunications Capability to All Americans in a Reasonable and Timely Fashion, GN Docket No. 17-199,” May 202. [Online]. Available: https://ecfsapi.fcc.gov/file/109212496527376/FINAL_Deere%20Comments%20on%20Section%20706%20NOI.pdf
- [5] S. Pitla, S. Bajwa, S. Bhusal *et al.*, “Ground and aerial robots for agricultural production: Opportunities and challenges,” *Council for Agricultural Science and Technology Issue Paper*, vol. IP70, 2020.
- [6] FCC Precision Ag Connectivity Task Force, “Task force for reviewing the connectivity and technology needs of precision agriculture in the united states,” Federal Communications Commission, Tech. Rep., Nov. 2021, <https://www.fcc.gov/sites/default/files/precision-ag-report-11102021.pdf>.
- [7] 3GPP TR 38.101-2, “User Equipment (UE) radio transmission and reception; Part 2: Range 2 Standalone (Release 17),” Sept. 2021. [Online]. Available: <https://www.3gpp.org/DynaReport/38-series.htm>
- [8] 3GPP, “Study on channel model for frequencies from 0.5 to 100 GHz (3GPP TR 38.901 version 16.1.0 Release 16),” Jan. 2020. [Online]. Available: <http://www.etsi.org/standards-search>
- [9] G. R. MacCartney and T. S. Rappaport, “Rural macrocell path loss models for millimeter wave wireless communications,” *IEEE J. Sel. Areas Commun.*, vol. 35, no. 7, pp. 1663–1677, 2017.
- [10] M. Rodriguez, R. Feick, H. Carrasco, R. Valenzuela, M. Derpich, and L. Ahumada, “Wireless access channels with near-ground level antennas,” *IEEE Trans. Commun.*, vol. 11, no. 6, pp. 2204–2211, 2012.
- [11] A. Torabi and S. A. Zekavat, “Near-ground channel modeling for distributed cooperative communications,” *IEEE Trans. Antennas Propag.*, vol. 64, no. 6, pp. 2494–2502, 2016.
- [12] S. B. Idso, R. D. Jackson, and R. J. Reginato, “Remote-sensing of crop yields: Canopy temperature and albedo measurements have been quantitatively correlated with final harvests of wheat.” *Science*, vol. 196, no. 4285, pp. 19–25, 1977.
- [13] M. C. Dobson and F. T. Ulaby, “Preliminary Evaluation of the SIR-B Response to Soil Moisture, Surface Roughness, and Crop Canopy Cover,” *IEEE Trans. Geosci. Remote Sens.*, vol. GE-24, no. 4, pp. 517–526, 1986.
- [14] A. Silva and M. Vuran, “Communication with aboveground devices in wireless underground sensor networks: An empirical study,” in *IEEE International Conference on Communications*, 2010.
- [15] X. Dong and M. Vuran, “A channel model for wireless underground sensor networks using lateral waves,” in *GLOBECOM - IEEE Global Telecommunications Conference*, 2011.
- [16] A. Salam, M. C. Vuran, and S. Irmak, “A statistical impulse response model based on empirical characterization of wireless underground channels,” *IEEE Transactions on Wireless Communications*, vol. 19, no. 9, pp. 5966–5981, sep 2020.
- [17] M. C. Vuran, M. M. Lunar, S. Nie, Y. Ge, S. Pitla, G. Bai, and C. E. Koksal, “Millimeter-Wave Agricultural Channel Measurements in Corn and Soybean Fields at Different Growth Stages,” in *IEEE International Symposium on Antennas and Propagation and USNC-URSI Radio Science Meeting*, July 2022.
- [18] A. Shkel, A. Mehrabani, and J. Kusuma, “A Configurable 60GHz Phased Array Platform for Multi-Link mmWave Channel Characterization,” in *2021 IEEE ICC Workshops*, 2021, pp. 1–6.
- [19] Telecom Infra Project, “TIP Channel Sounder Program Results Summary Report,” 2020. [Online]. Available: <https://telecominfraproject.com/mmwave/>
- [20] ITU, “Recommendation P.833-10, Attenuation in Vegetation,” Sept. 2021.
- [21] ———, “Recommendation ITU-R P.676-12, Attenuation by atmospheric gases and related effects,” Aug. 2019. [Online]. Available: <https://www.itu.int/rec/R-REC-P.676-12-201908-I/en>
- [22] C. F. Bohren and B. A. Albrecht, *Atmospheric Thermodynamics*. New York, NY: Oxford University Press, 1st edition, 1998.
- [23] S. Ju, O. Kanhere, Y. Xing, and T. S. Rappaport, “A millimeter-wave channel simulator NYUSIM with spatial consistency and human blockage,” in *2019 IEEE GLOBECOM*. IEEE, 2019, pp. 1–6.
- [24] E. Zöchmann, K. Guan, and M. Rupp, “Two-ray models in mmWave communications,” in *2017 IEEE 18th SPAWC*, 2017, pp. 1–5.
- [25] H. T. Fry, “The emergence of the Beaufort Scale,” *The Mariner’s Mirror*, vol. 53, no. 4, pp. 311–313, 1967.